RESEARCH ARTICLE

NOTCH Decoys That Selectively Block DLL/NOTCH or JAG/NOTCH Disrupt Angiogenesis by Unique Mechanisms to Inhibit Tumor Growth

Thaned Kangsamaksin[1,2], Aino Murtomaki[1,3], Natalie M. Kofler[1], Henar Cuervo[1], Reyhaan A. Chaudhri[1], Ian W. Tattersall[1], Paul E. Rosenstiel[4], Carrie J. Shawber[1,5,6], and Jan Kitajewski[1,4,5]

ABSTRACT A proangiogenic role for Jagged (JAG)-dependent activation of NOTCH signaling in the endothelium has yet to be described. Using proteins that encoded different NOTCH1 EGF-like repeats, we identified unique regions of Delta-like ligand (DLL)–class and JAG-class ligand–receptor interactions, and developed NOTCH decoys that function as ligand-specific NOTCH inhibitors. $N1_{10-24}$ decoy blocked JAG1/JAG2–mediated NOTCH1 signaling, angiogenic sprouting *in vitro*, and retinal angiogenesis, demonstrating that JAG-dependent NOTCH signal activation promotes angiogenesis. In tumors, $N1_{10-24}$ decoy reduced angiogenic sprouting, vessel perfusion, pericyte coverage, and tumor growth. JAG–NOTCH signaling uniquely inhibited expression of antiangiogenic soluble (s) VEGFR1/sFLT1. $N1_{1-13}$ decoy interfered with DLL1–DLL4-mediated NOTCH1 signaling and caused endothelial hypersprouting *in vitro*, in retinal angiogenesis, and in tumors. Thus, blockade of JAG- or DLL-mediated NOTCH signaling inhibits angiogenesis by distinct mechanisms. JAG–NOTCH signaling positively regulates angiogenesis by suppressing sVEGFR1–sFLT1 and promoting mural–endothelial cell interactions. Blockade of JAG-class ligands represents a novel, viable therapeutic approach to block tumor angiogenesis and growth.

SIGNIFICANCE: This is the first report identifying unique regions of the NOTCH1 extracellular domain that interact with JAG-class and DLL-class ligands. Using this knowledge, we developed therapeutic agents that block JAG-dependent NOTCH signaling and demonstrate for the first time that JAG blockade inhibits experimental tumor growth by targeting tumor angiogenesis. *Cancer Discov; 5(2); 182–97. ©2014 AACR.*

See related commentary by Briot and Iruela-Arispe, p. 112.

[1]Department of Obstetrics/Gynecology, Columbia University Medical Center, Columbia University, New York, New York. [2]Department of Biochemistry, Faculty of Science, Mahidol University, Bangkok, Thailand. [3]Division of Genetics, Department of Biosciences, Viikki Biocenter, University of Helsinki, Helsinki, Finland. [4]Department of Pathology and Cellular Biology, Columbia University Medical Center, Columbia University, New York, New York. [5]Herbert Irving Comprehensive Cancer Center, Columbia University Medical Center, Columbia University, New York, New York. [6]Department of Surgery, Columbia University Medical Center, Columbia University, New York, New York.

Note: Supplementary data for this article are available at Cancer Discovery Online (http://cancerdiscovery.aacrjournals.org/).

Corresponding Author: Jan Kitajewski, Columbia University Medical Center, Irving Cancer Research Center, Columbia University, 1130 Saint Nicholas Avenue, ICRC 926, New York, NY 10032. Phone: 212-851-4688; Fax: 212-851-4504; E-mail: jkk9@columbia.edu

doi: 10.1158/2159-8290.CD-14-0650

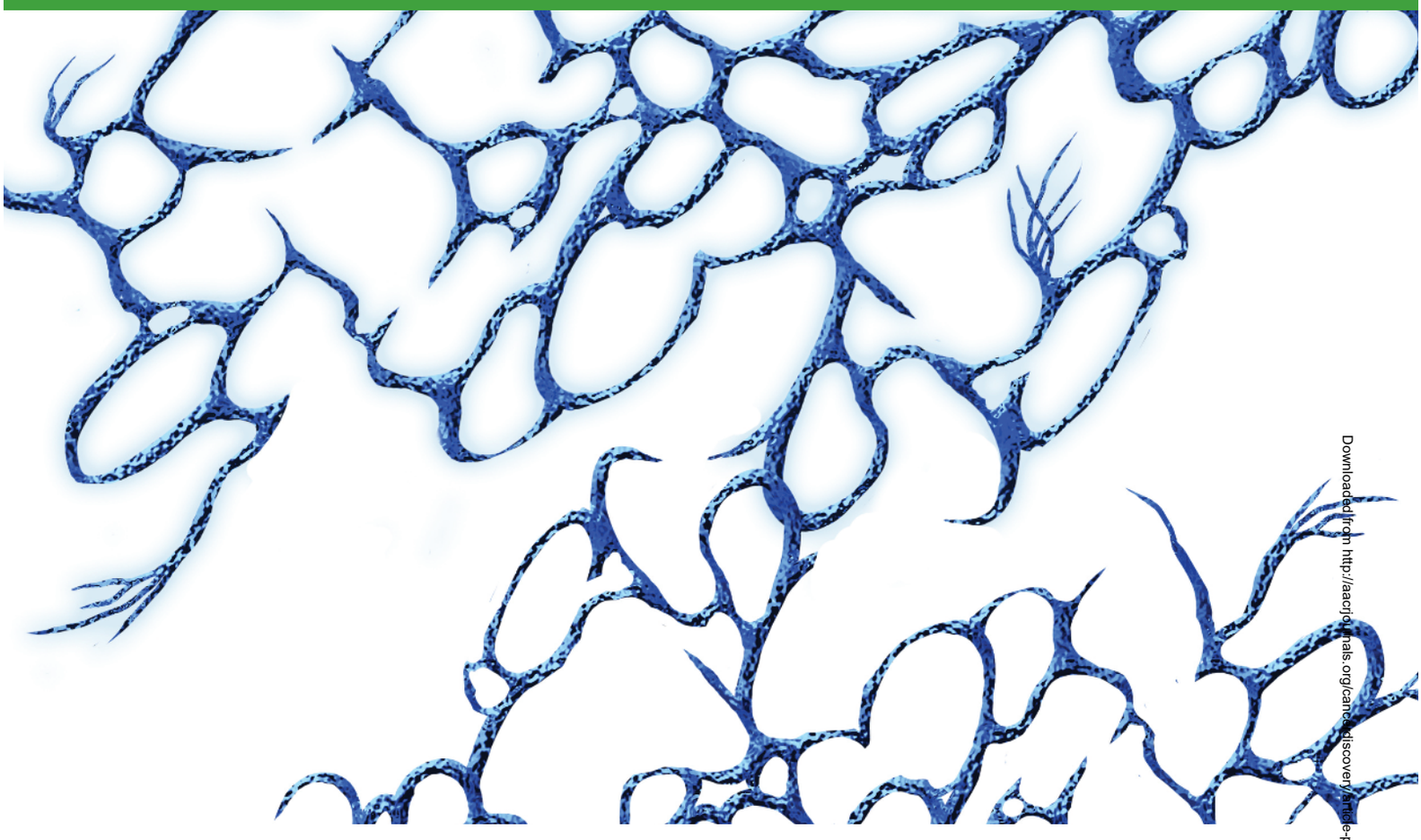

INTRODUCTION

Tumor angiogenesis is regulated by a variety of signaling pathways, some of which are validated targets of antiangiogenic therapies. Molecular and genetic studies reveal that NOTCH signaling regulates cell fate, proliferation, differentiation, and apoptosis, depending on the cellular context. In the endothelium, Delta-like 4 (DLL4)–NOTCH signaling suppresses endothelial cell proliferation, migration, and sprouting (1–3). Agents that block gamma-secretase activity, required for NOTCH signal activation, or that block DLL4, disrupt tumor angiogenesis (4–6) but have toxicities that may limit their utility (5–7).

NOTCH proteins and their ligands interact on neighboring cells requiring direct cell–cell contact. The highly conserved mammalian *NOTCH* gene family encodes transmembrane receptors NOTCH1, NOTCH2, NOTCH3, and NOTCH4. The ligands for NOTCH are transmembrane proteins of two classes: Jagged ligands (JAG) JAG1 and JAG2, and Delta-like ligands (DLL) DLL1, DLL3, and DLL4. Upon ligand activation, a cleaved NOTCH intracellular domain is released by a gamma-secretase–dependent proteolytic cleavage and transits to the nucleus, where it converts the CBF1, Suppressor of Hairless, LAG-1 (CSL) transcriptional repressor to an activator (8). The human NOTCH1 extracellular domain comprises 36 EGF-like repeats. NOTCH ligands share a conserved degenerate EGF-like repeat, the Delta/Serrate/LAG-2 (DSL) domain, which is required for ligand binding to NOTCH (9, 10), followed by an EGF-like repeat region that varies; JAGs have 16 EGF-like repeats, and DLLs contain 8 or fewer. NOTCH EGF-like repeats 11 and 12 and the DSL domain of ligands are necessary for NOTCH interaction with all ligands (11, 12). It is unknown whether there are distinct NOTCH EGF-like repeats that interact with DLL-class versus JAG-class ligands, and this gap in knowledge has limited our understanding of ligand-specific interactions that elicit unique NOTCH signaling outcomes.

NOTCH proteins and ligands are upregulated in several cancers, and the roles of NOTCH signaling in tumor cells include both tumor-promoting and tumor-suppressing activities, depending on the tumor type (13, 14). Previous studies have established a key role for DLL4–NOTCH signaling in tumor angiogenesis, as reviewed in ref. 15. DLL4 blockade inhibits tumor growth by dysregulating tumor angiogenesis, characterized by increased endothelial cell proliferation and a hypersprouted but nonfunctional tumor vasculature (5, 6). DLL4/NOTCH function in angiogenesis involves an intricate cross-regulation of NOTCH and VEGF signaling pathways. VEGF induces expression of NOTCH1, NOTCH4, and DLL4 (16–18). NOTCH activation reduces expression of VEGFR2 but increases expression of VEGFR1 (19, 20). In endothelial cells, VEGFR3 can be either induced (20, 21) or

reduced (22) by NOTCH signaling. In murine retinal angiogenesis, DLL4 and JAG1 have unique activities in the endothelium, as loss-of-function experiments result in distinct phenotypes. DLL4 heterozygotes display angiogenic hypersprouting, whereas endothelial-specific loss of JAG1 impairs retinal angiogenesis (23, 24).

We have created soluble NOTCH inhibitors consisting of different EGF-like repeats of the NOTCH1 extracellular domain fused to human IgG Fc (NOTCH1 decoy). A human NOTCH1 decoy with all 36 EGF-like repeats functioned similarly to a rat NOTCH1 decoy that inhibits JAG1, DLL1, and DLL4 (25). We asked whether NOTCH1 decoys that incorporate distinct NOTCH1 EGF-like repeats would differentially antagonize NOTCH ligand classes. NOTCH1 decoy variants were identified that selectively inhibited DLL-class versus JAG-class NOTCH ligands, providing the first delineation of ligand-specific interaction domains in human NOTCH1. NOTCH1 decoy variants were evaluated for effects on *in vitro*, retinal, and tumor angiogenesis. A NOTCH1 decoy variant that interferes with JAG1 and JAG2 reduced NOTCH1 signaling, blocked angiogenic growth in retinas and tumors, and reduced tumor growth. Furthermore, JAG blockade specifically increased antiangiogenic soluble VEGFR1 (sVEGFR1/sFLT1) levels and disrupted pericyte coverage, providing a mechanism by which JAG blockade disrupts tumor growth. A NOTCH1 decoy variant that interfered with DLL1 and DLL4 caused a hypersprouting phenotype, promoted dysfunctional tumor angiogenesis, and inhibited tumor growth.

RESULTS

NOTCH1 Decoy Variants Define Unique JAG and DLL Interaction Domains

We developed a human NOTCH1 decoy ($N1_{1–36}$ decoy), encoding the 36 extracellular EGF-like repeats of human NOTCH1 fused to human IgGγ heavy chain (Fc) and variants consisting of EGF-like repeats 1 to 13 ($N1_{1–13}$) or 1 to 24 ($N1_{1–24}$; Fig. 1A) and tested their ability to interfere with ligand-specific NOTCH activation. These N1 decoy variants were secreted from 293T cells into the media (Fig. 1B). The inhibitory activity against specific NOTCH ligands, DLL4 and JAG1, was assessed using a NOTCH/CSL reporter assay. HeLa cells expressing either DLL4 or JAG1, and individual N1 decoy variants or Fc, were cocultured with HeLa cells expressing full-length rat NOTCH1 and a CSL-luciferase reporter. Compound E, a gamma-secretase inhibitor (GSI), was used as a control for NOTCH1 signal inhibition at a concentration of 200 nmol/L. Expression of $N1_{1–24}$ and $N1_{1–36}$ decoys significantly blocked both DLL4- and JAG1-induced NOTCH1 signaling (Fig. 1C and D). $N1_{1–13}$ decoy inhibited DLL4-induced NOTCH1 signaling but not JAG1-mediated NOTCH1 signaling (Fig. 1C and D). Thus, $N1_{1–24}$ and $N1_{1–36}$ decoys acted as pan-ligand inhibitors, blocking both DLL4 and JAG1, whereas $N1_{1–13}$ decoy inhibited only DLL4 and was insufficient for blocking JAG1.

Based upon the activity of $N1_{1–13}$ decoy, we hypothesized that EGF-like repeats downstream of repeat 13 have a role in productive JAG1–NOTCH1 signaling, and thus created $N1_{10–24}$ and $N1_{10–36}$ decoy variants (Fig. 1E). It has been demonstrated that EGF-like repeats 11 and 12 are necessary for functional and physical interaction between NOTCH and its ligands (11, 26). To further assess the importance of EGF-like repeats 11 and 12, we generated N1 decoys encoding EGF-like repeats 14 to 24 ($N1_{14–24}$) and 14 to 36 ($N1_{14–36}$). These N1 decoy variants were secreted from 293T cells (Fig. 1F). We probed for their inhibitory activity against DLL4–NOTCH1 and JAG1–NOTCH1 signaling. $N1_{10–24}$ and $N1_{10–36}$ decoys did not inhibit DLL4-mediated NOTCH1 signaling, indicating that EGF-like repeats 1 to 9 are required for DLL4–NOTCH interactions (Fig. 1G). In contrast, $N1_{10–24}$ decoy significantly blocked JAG1-induced NOTCH1 signaling (Fig. 1H). $N1_{10–36}$ decoy did not inhibit JAG1, possibly due to its poor secretion. $N1_{14–24}$ and $N1_{14–36}$ decoys did not block NOTCH1 signaling via either DLL4 or JAG1 (Fig. 1G and H), demonstrating that EGF-like repeats 10 to 13 are critical for JAG1–NOTCH interaction. We broadened our analysis to include all known activating NOTCH ligands. We found that $N1_{1–13}$ decoy blocked DLL1–NOTCH1 signaling (Supplementary Fig. S1A) but not JAG2–NOTCH1 signaling (Supplementary Fig. S1B). $N1_{10–24}$ decoy did not block DLL1–NOTCH1 signaling (Supplementary Fig. S1C) and blocked JAG2–NOTCH1 signaling (Supplementary Fig. S1D). $N1_{1–24}$ decoy and $N1_{1–36}$ inhibited both DLL1 and JAG2 activation of NOTCH1 (Supplementary Fig. S1A and S1B). Thus, ligand specificity for $N1_{1–13}$ decoy and $N1_{10–24}$ decoy was also observed with DLL1 and JAG2.

A dose–response analysis of $N1_{1–13}$ decoy protein purified from conditioned media produced by Chinese hamster ovary (CHO) cell clones showed that $N1_{1–13}$ decoy preferentially inhibited DLL4 activation of NOTCH1, and inhibited JAG1 activation of NOTCH1 only at a high dose of 50 μg/mL (Supplementary Fig. S2A and S2B). $N1_{1–24}$ decoy protein was able to inhibit both DLL4 and JAG1 activation of NOTCH1 at all concentrations (Supplementary Fig. S2C and S2D). Thus, at high doses, the $N1_{1–13}$ decoy was less discriminatory, which is consistent with the role of NOTCH1 EGF-like repeats 11 and 12 in interactions with DLL and JAG ligands. We conclude that $N1_{1–13}$ decoy functions as a dose-dependent, selective DLL-class ligand inhibitor, and $N1_{10–24}$ decoy functions as a JAG-class ligand inhibitor.

To confirm binding specificity, N1 decoys and full-length FLAG-tagged NOTCH ligands DLL4 and JAG1 were coexpressed in 293T cells and coimmunoprecipitations performed (Fig. 2A). $N1_{1–13}$ decoy coimmunoprecipitated with DLL4, but not JAG1. $N1_{10–24}$ decoy coimmunoprecipitated with JAG1, but not DLL4. $N1_{1–24}$ decoy coimmunoprecipitated with both DLL4 and JAG1. Similar ligand specificity of the decoys was observed when binding assays were done with soluble ligands lacking transmembrane and cytoplasmic domains (Supplementary Fig. S3). Full-length NOTCH1 did not coimmunoprecipitate with N1 decoys (Fig. 2B), demonstrating that N1 decoys do not bind receptors. We conclude that N1 decoys function to block ligand-specific NOTCH signaling by competitively binding the extracellular domains of DLL-class or JAG-class ligands.

NOTCH1 Decoy Variants Have Unique Effects on Angiogenesis *In Vitro*

To determine the angiogenic effects of N1 decoys, we used an *in vitro* angiogenesis assay in which human umbilical vein endothelial cell (HUVEC)–coated collagen/dextran beads are

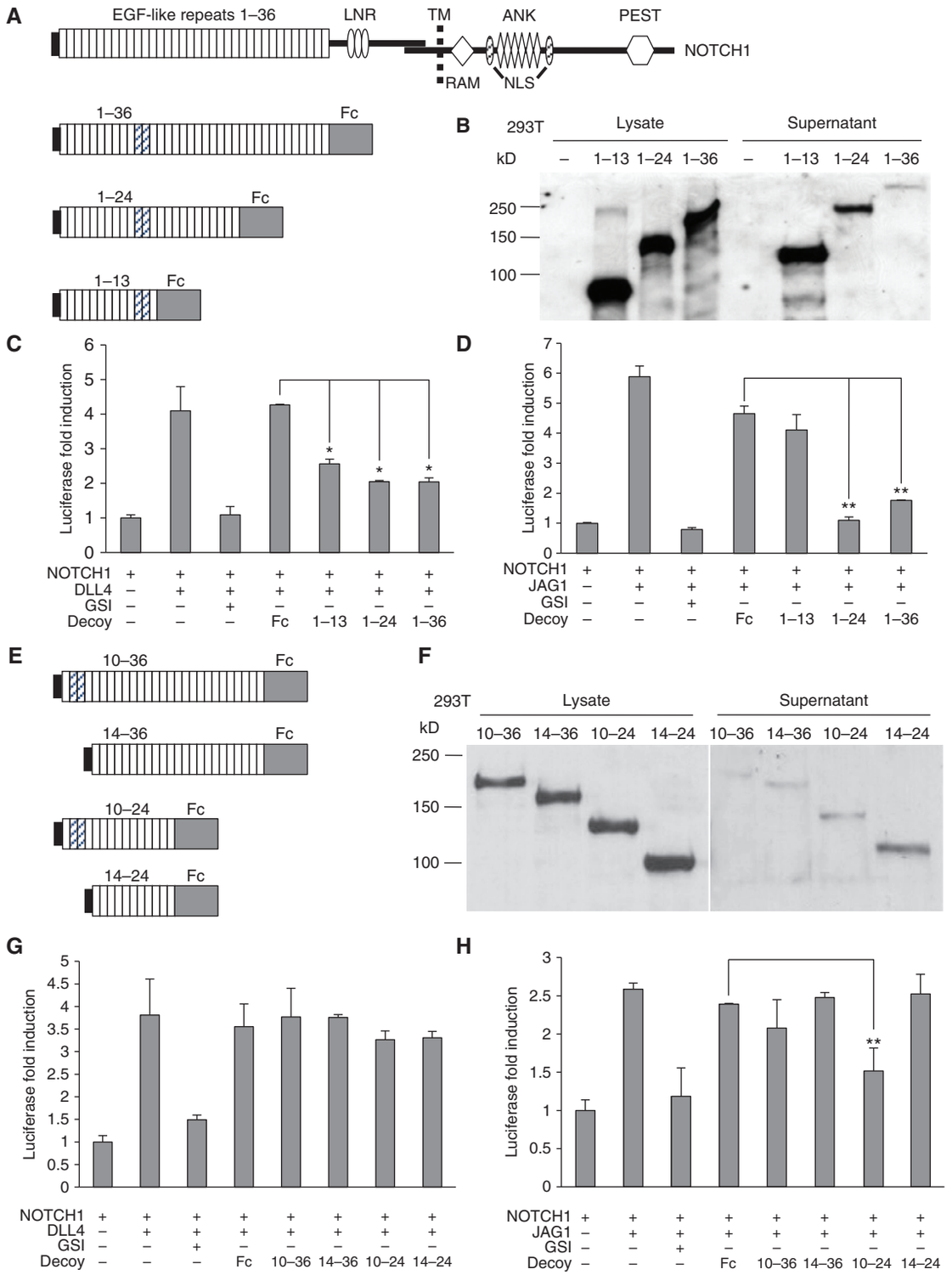

Figure 1. N1 decoys differently inhibit ligand-induced NOTCH signaling. **A** and **E,** schematic of NOTCH1 decoy variants. **A,** NOTCH1 protein: EGF-like repeats 11 and 12 indicated with shading. LNR, LIN-12/NOTCH repeats; TM, transmembrane domain; RAM, CSL interaction domain; ANK, ankyrin repeats; NLS, nuclear location signal; PEST, proline-, glutamic acid–, serine-, threonine-rich sequence. EGF-like repeats 1 to 36 of human NOTCH1 ($N1_{1-36}$), repeats 1 to 24 ($N1_{1-24}$), or repeats 1 to 13 ($N1_{1-13}$) are fused in frame with human IgG Fc. **E,** EGF-like repeats 10 to 36 of human NOTCH1 ($N1_{10-36}$), repeats 14 to 36 ($N1_{14-36}$), repeats 10 to 24 ($N1_{10-24}$), or repeats 14 to 24 ($N1_{14-24}$) are fused in frame with human IgG Fc. EGF-like repeats 11 and 12 indicated with shading. **B** and **F,** N1 decoy variants expressed in 293T cells detected from total cell lysates and supernatant by immunoblotting with an anti-human Fc antibody. **C, D, G,** and **H,** NOTCH signal activation measured in HeLa cells expressing full-length rat NOTCH1, N1 decoys, and 11CSL-Luc cocultured with HeLa cells expressing NOTCH ligands. Coculture assays were performed in triplicate and repeated three times. Mean luciferase fold induction ± SD; *, $P < 0.002$ and **, $P < 0.005$.

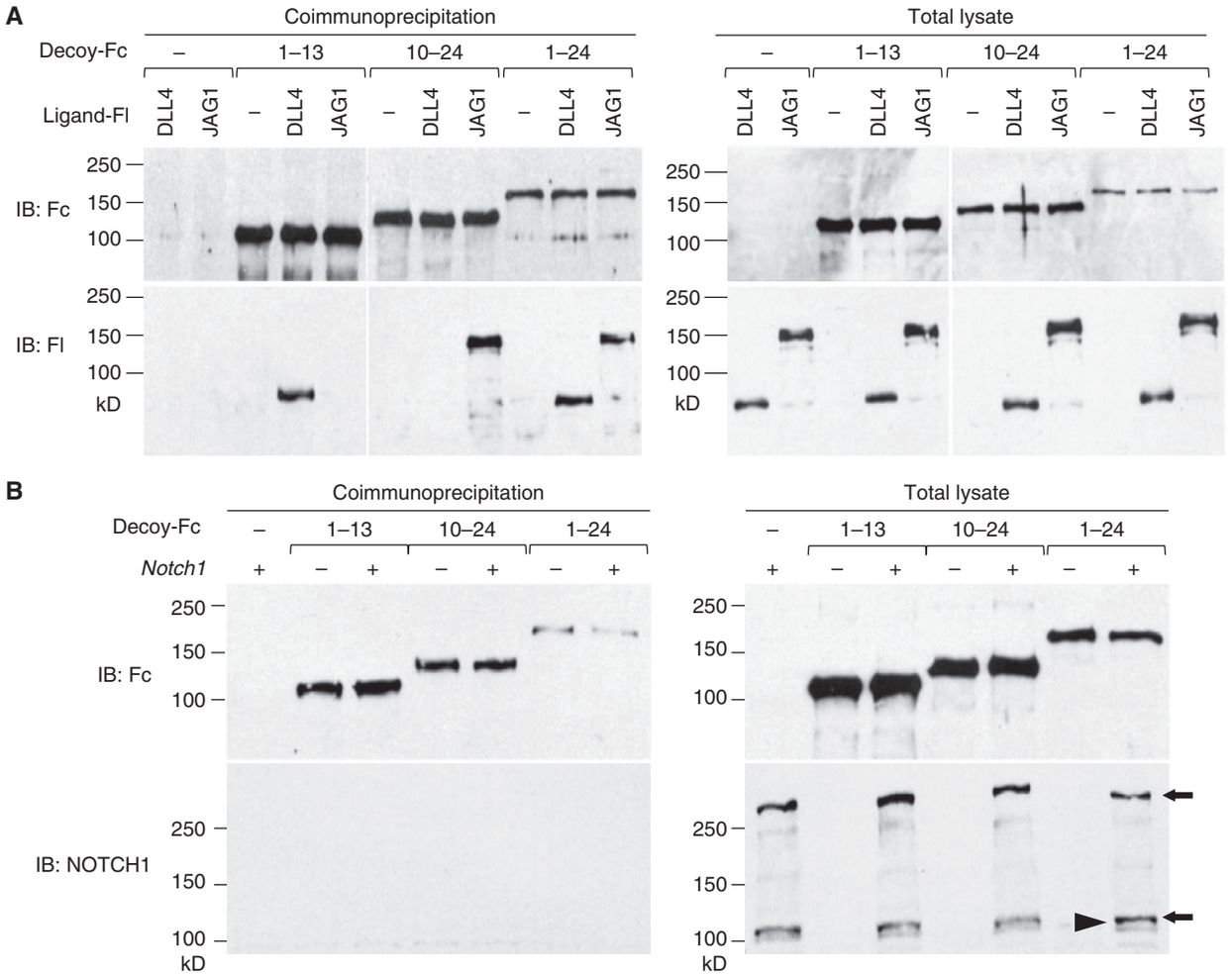

Figure 2. N1 decoy variants demonstrate ligand-specific binding. **A,** N1 decoys and FLAG (Fl)-tagged DLL4 or JAG1 were cotransfected in 293T cells. Lysates immunoprecipitated with anti-Fc or anti-FLAG antibodies or total cell lysates were immunoblotted with anti-Fc or anti-FLAG antibody. **B,** N1 decoys and full-length rat NOTCH1 were cotransfected in 293T cells. Lysates immunoprecipitated with anti-Fc or anti-NOTCH1 antibodies or total cell lysates were immunoblotted with anti-Fc or anti-NOTCH1 antibody. Anti-NOTCH1 antibody recognizes full-length rat NOTCH1 and furin-cleaved rat NOTCH1 (arrows) as well as endogenous furin-cleaved human NOTCH1 (arrowhead). These assays were repeated twice.

embedded in fibrin (27). In response to angiogenic factors secreted by a fibroblast feeder layer, HUVECs sprout from the bead to form branched, lumenized sprouts. The sprouts formed by HUVECs expressing Fc or N1 decoys were evaluated on day 7. In the Fc control, endothelial cell sprouts merged to form multicellular, branched, and lumen-containing vascular networks (Fig. 3A). HUVECs expressing $N1_{1–13}$ decoy had a hypersprouting phenotype characterized by increased branch points, as seen by a 76% increase in the number of branch points over control (Fig. 3A and B). The $N1_{1–13}$ decoy phenotype is consistent with attenuation of DLL4–NOTCH signaling, as has been shown using an anti-DLL4 antibody (5). In contrast, HUVECs expressing $N1_{10–24}$ and $N1_{1–24}$ decoys showed reduced network formation compared with control (Fig. 3A and B). $N1_{10–24}$ and $N1_{1–24}$ decoy HUVECs exhibited stunted sprouts and a 40% and 68% decrease in the number of branch points, respectively (Fig. 3B). Thus, JAG blockade resulted in an antiangiogenic response, and this effect dominated over DLL inhibition when using the pan-ligand inhibitor $N1_{1–24}$ decoy.

NOTCH1 Decoy Variants Have Unique Effects on Murine Retinal Angiogenesis

To determine how ligand-specific NOTCH inhibition affects developmental angiogenesis, we assessed N1 decoy treatment during murine retinal angiogenesis, where DLL4/NOTCH function is well understood (2, 3). The effects of circulating N1 decoys on target tissues were assessed using injected adenoviruses that expressed N1 decoy proteins. To deliver N1 decoy to the bloodstream, adenovirus vectors expressing N1 decoys or Fc were injected into murine neonates, leading to hepatocyte infection and decoy secretion into circulation. All N1 decoys were detected in serum by Western blot analysis at time of retina collection (Supplementary Fig. S4). $N1_{1–13}$ decoy significantly increased retinal vascular density (Fig. 3C and D), consistent with the increase in tip cells typical of

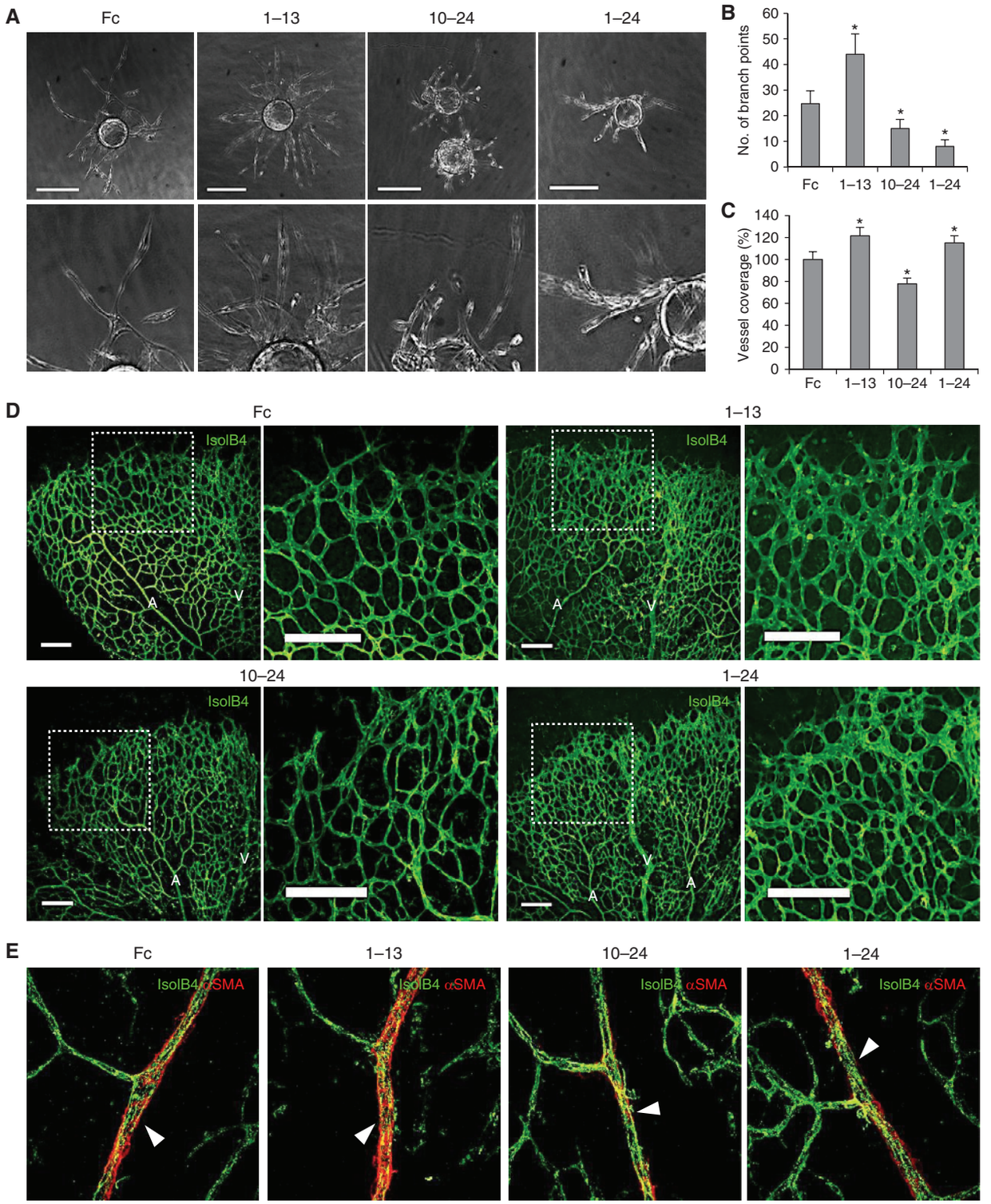

Figure 3. N1 decoys variants function distinctly *in vitro* and in retinal angiogenesis. **A,** N1 decoy assessment in the HUVEC fibrin bead sprouting assay at day 7; scale bars, 200 μm. **B,** quantification of the mean number of branch points per bead ± SD; *, $P < 0.05$. Fibrin bead sprouting assays were performed in triplicate and repeated twice. **C,** quantification of the mean percentage of vascular density of the P5 retinas ± SD; *, $P < 0.05$. **D,** isolectin B4 (IsolB4) staining of P5 retinas; A, artery; V, vein. Scale bars, 100 μm. **E,** isolectin B4 (IsolB4) and αSMA staining of P5 retinas. Vascular smooth muscle cell–covered retinal arteries noted with arrowheads ($n = 6$).

DLL4 inhibition (Figs. 1C and D and 3A). In contrast, $N1_{10–24}$ decoy reduced blood vessel density in the retina (Fig. 3C and D). $N1_{1–24}$ decoy increased retinal vasculature density (Fig. 3C and D), indicating that it predominantly functions as a DLL4 antagonist in murine retinal angiogenesis. This is in contrast with the predominant function of $N1_{1–24}$ decoy during *in vitro* sprouting, in which it acts as a JAG antagonist (Fig. 3A and B).

JAG1 plays a role in recruitment of vascular smooth muscle cells to arteries (23, 24), a role that we evaluated in retinas of mice treated with N1 decoys. A decrease in α-smooth muscle actin (αSMA)–expressing vascular smooth muscle cell coverage was observed in neonate retinas on the arteries in $N1_{10–24}$ and $N1_{1–24}$ decoy–treated groups (Fig. 3E, quantified in Supplementary Fig. S5A), a phenotype also seen in endothelial-specific *Jag1*-mutant mice (23, 24). Vascular smooth muscle cell coverage of the $N1_{1–13}$ decoy–treated group was similar to the Fc-treated group, indicating that, whereas the effect of $N1_{1–24}$ decoy on sprouting represents DLL signaling inhibition, its effect on smooth muscle cell coverage represents JAG signaling inhibition. No significant effects on smooth muscle cell coverage were observed when the N1 decoys were administered to adult mice (Supplementary Fig. S5B), suggesting that the effect of decoy-mediated inhibition is limited to periods of active angiogenesis.

NOTCH1 Decoys Inhibit Tumor Growth and Angiogenesis by Unique JAG-Dependent versus DLL-Dependent Mechanisms

Previous work has shown that NOTCH inhibition can disrupt tumor growth and angiogenesis (5, 6, 25, 28, 29). However, ligand class–specific blockade has yet to be assessed. We hypothesized that the diverse ligand-inhibitory activities of N1 decoy variants would have distinct antiangiogenic and antioncogenic efficacies.

We tested the *in vitro* effects of N1 decoys ($N1_{1–13}$, $N1_{10–24}$, and $N1_{1–24}$ decoys) on colony formation, proliferation, and apoptosis of four different tumor cell lines, Mm5MT-FGF4 (mouse mammary tumor; ref. 25), KP1-VEGF (human pancreatic tumor; ref. 25), LLC (mouse lung tumor), and B16-F10 (mouse melanoma). All N1 decoys significantly inhibited colony formation of Mm5MT-FGF4 cells in a soft-agar assay, but not other tumor cell lines (Supplementary Fig. S6A and S6B). Thus, N1 decoys have the potential to inhibit both Mm5MT-FGF4 tumor cells and host cells. N1 decoys did not affect tumor cell proliferation or apoptosis in any of the tumor lines grown in monolayer cultures (Supplementary Fig. S6C and S6D).

To evaluate N1 decoys in tumors *in vivo*, we performed xenograft studies using the four different tumor cell lines. Our goal was to evaluate N1 decoys as therapeutic proteins. The adenoviral expression system was used to allow N1 decoy proteins to be delivered to tumors, simulating the effects of protein delivery via circulation. Adenoviruses encoding N1 decoys were administered to nude mice 3 days after subcutaneous tumor implantation, and decoy proteins were detected in the serum from 2 days after injection until time of sacrifice at day 21 (Supplementary Fig. S7A). Using a human Fc ELISA, we found varying serum levels of N1 decoys, with the larger $N1_{1–24}$ and $N1_{1–36}$ decoys secreted into the serum at lower levels than the $N1_{1–13}$ and $N1_{10–24}$ decoys (Supplementary Fig. S7B). All N1 decoys tested significantly decreased growth of Mm5MT-FGF4, LLC, and B16-F10 tumors, whereas only $N1_{10–24}$ and $N1_{1–24}$ decoys inhibited the growth of KP1–VEGF tumors (Fig. 4A).

We sought to determine how blockade of DLL-class versus JAG-class NOTCH ligands affected tumor angiogenesis, and found that the different N1 decoys had distinct effects. $N1_{1–13}$ decoy significantly increased endothelial cell density in all tumor models (Fig. 4B and C), similar to the effect seen with DLL4 blockade (5). In contrast, tumors from the $N1_{10–24}$ and $N1_{1–24}$ decoy groups had decreased endothelial cell density (Fig. 4B and C). In the Mm5MT-FGF4 model, vessel perfusion was determined by lectin perfusion followed by endomucin staining of the tumor endothelium. The different N1 decoys all caused reduced tumor perfusion in Mm5MT-FGF4 tumors, with perfusion relative to control decreased 72% ($N1_{1–13}$), 90% ($N1_{10–24}$), and 84% ($N1_{1–24}$; Fig. 5A). Consistent with poor perfusion, N1 decoy–treated tumors had increased hypoxia (Fig. 5B). Tumor perfusion and hypoxia were quantified (Fig. 5C and D) and were found to be significantly different from control. To evaluate vessel regression, tumors were immunostained for endomucin and collagen IV, to detect areas where a collagen sleeve remains after endothelial degeneration. Collagen IV deposition was increased in $N1_{1–13}$ decoy–treated tumors and reduced in $N1_{10–24}$ and $N1_{1–24}$ decoy tumors (Fig. 5E). When normalized to endomucin staining, however, there was no difference between Fc groups and N1 decoy–treated groups (Fig. 5F), indicating that the reduced tumor vasculature in $N1_{10–24}$ and $N1_{1–24}$ decoy tumors was not due to vessel regression. We conclude that blockade of DLL-class versus JAG-class NOTCH ligands had opposing effects on tumor vessel density, but uniformly reduced tumor perfusion and increased hypoxia. In tumor angiogenesis, $N1_{1–24}$ decoy behaved as a JAG-class inhibitor, consistent with the results when assessed *in vitro* (Fig. 3A and B).

As N1 decoys affected mural cell coverage during retinal angiogenesis (Fig. 3E), we evaluated mural cell coverage of N1 decoy–treated Mm5MT-FGF4 tumor vasculature, which is rich in NG2-positive pericytes. Tumor sections were immunostained for endomucin and NG2 or αSMA to visualize pericytes and vascular smooth muscle cells, respectively. Relative to the Fc group, $N1_{1–13}$ decoy did not alter pericyte–endothelial association, and pericyte vascular coverage was unchanged (Fig. 5G and H). In Fc tumors, NG2-positive pericytes were closely associated with endothelial cells (Fig. 5H). In contrast, pericytes were disassociated from endothelial cells in $N1_{10–24}$ and $N1_{1–24}$ decoy–treated tumors (Fig. 5H). $N1_{1–13}$ decoy–treated tumors showed increased overall presence of NG2-positive cells, whereas $N1_{10–24}$ and $N1_{1–24}$ decoy–treated tumors showed decreased overall NG2-positive cells (Supplementary Fig. S8A). When normalized to endothelial content, $N1_{10–24}$ decoy–treated tumors alone displayed reduced pericyte vascular coverage relative to control (Fig. 5G). Assessment of larger vessels in the tumors revealed reduced vascular smooth muscle αSMA immunostaining in $N1_{10–24}$ and $N1_{1–24}$ decoy–treated tumors (Supplementary Fig. S8B and S8C). Thus, in tumor angiogenesis, DLL-class inhibition had no apparent effect on vascular mural cells, whereas blocking JAG-class ligands via $N1_{10–24}$ decoy resulted in defective pericyte and vascular smooth muscle cell coverage. $N1_{1–24}$ decoy resulted in

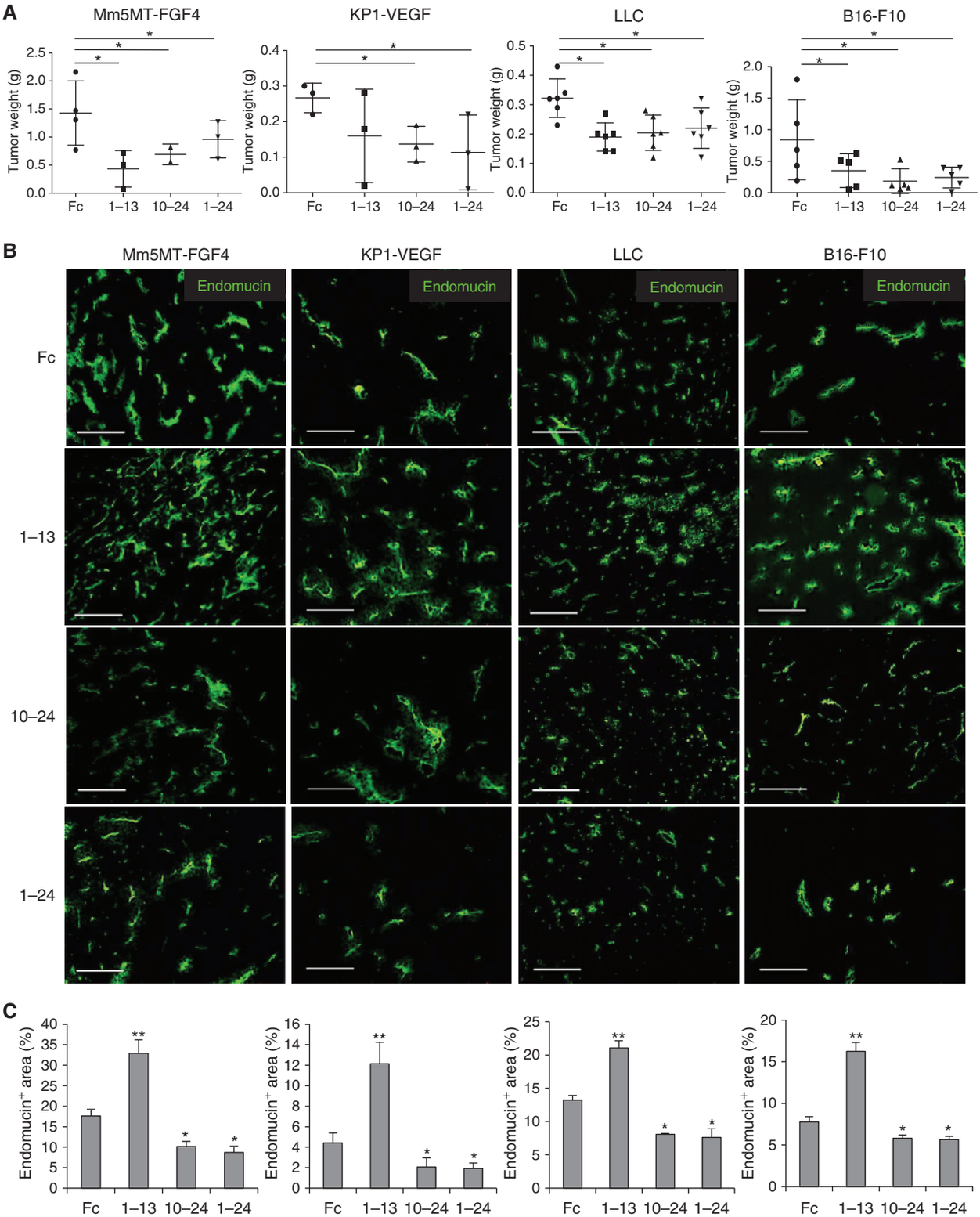

Figure 4. N1 decoys block xenograft tumor growth and disrupt tumor angiogenesis. **A,** Mm5MT-FGF4, KP1-VEGF, LLC, and B16-F10 tumors weigh significantly less in the N1 decoy–treated groups compared with the Fc control group. Tumor weight measured at the time of harvest. Data, as mean tumor weight ± SD; *, $P < 0.05$ ($n = 4$–5). **B,** endomucin staining of N1 decoy–treated Mm5MT-FGF4, KP1-VEGF, LLC, and B16-F10 tumors; scale bars, 30 μm. **C,** quantification of endomucin-positive vascular density. Data, mean percentage of the endomucin-positive area ± SD; *, $P < 0.003$; **, $P < 0.0005$ ($n = 4$–5).

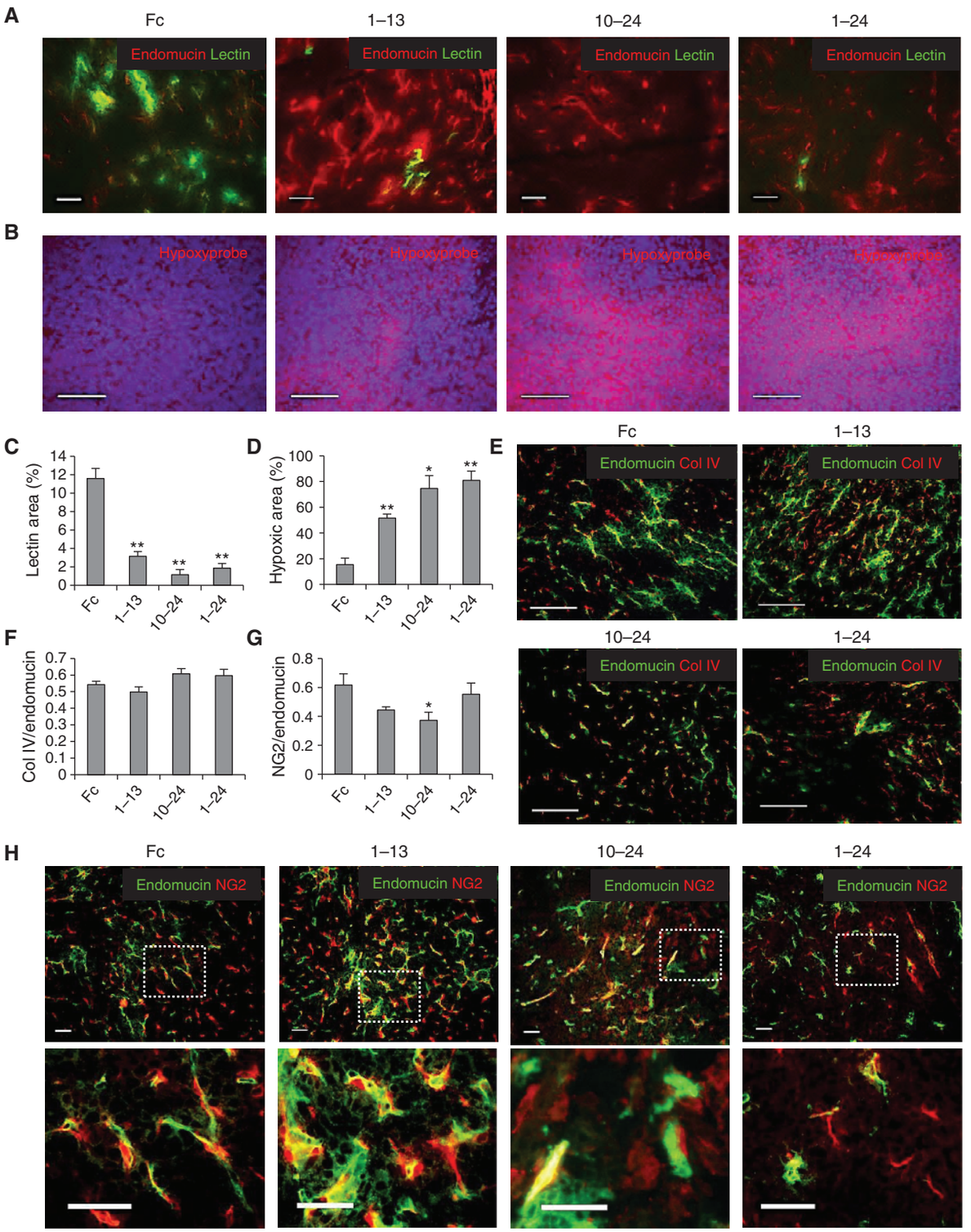

Figure 5. N1 decoys reduced perfusion and JAG-specific decoys disrupted pericyte association in Mm5MT-FGF4 tumors. **A,** endomucin staining of FITC-lectin perfused tumors. **B,** antibody detection of tumors from hypoxyprobe-injected mice and costained with 4,6-diamidino-2-phenylindole (DAPI). **C,** quantitation of vessel perfusion by the mean percentage of the lectin-positive area ± SD; *, $P < 0.006$ ($n = 4$–5). **D,** quantitation of the mean percentage of the hypoxyprobe-positive area ± SD; *, $P < 0.002$ and **, $P < 0.05$ ($n = 4$–5). **E,** collagen type IV (ColIV) and endomucin staining of Mm5MT-FGF4 tumor sections; **A, B,** and **E,** scale bars, 30 μm. **F,** quantification of the mean collagen type IV-positive area divided by the mean endomucin-positive area, ± SD; ($n = 4$–5). **G,** quantification of the mean NG2-positive area divided by the mean endomucin-positive area, ± SD; *, $P < 0.02$ ($n = 4$–5). **H,** endomucin and NG2 staining of Mm5MT-FGF4 tumor sections; scale bars, 10 μm.

defective mural cell coverage of tumor vessels, but did not reduce pericyte coverage, thus incompletely mimicking $N1_{10–24}$ decoy effects in tumor vasculature.

JAG and DLL Differentially Regulate sVEGFR1/Soluble FLT1

We explored the mechanisms by which DLL- and JAG-specific N1 decoy variants elicited their distinct effects in endothelial cells. HUVECs were infected with lentiviruses encoding Fc, $N1_{1–13}$, $N1_{10–24}$, or $N1_{1–24}$ decoys, and the effects on endothelial NOTCH downstream targets determined. Expression of $N1_{1–13}$, $N1_{10–24}$, and $N1_{1–24}$ decoys and JAG1 knockdown (J1KD) suppressed the expression of HEY1, HEYL, and HES1 (Fig. 6A), direct targets of NOTCH/CSL transactivation (30). Unlike N1 decoys that are able to block DLL-class ligands, neither $N1_{10–24}$ decoy nor J1KD reduced HEY2 transcripts (Fig. 6A).

NOTCH signaling regulates VEGF signaling in endothelial cells, largely through the regulation of VEGF receptor expression (15). Quantitative RT (qRT)-PCR and FACS was performed to determine the effect of N1 decoys or J1KD on VEGF receptors. In HUVEC, $N1_{1–13}$, $N1_{10–24}$, $N1_{1–24}$ decoys and J1KD increased VEGFR2 expression (Fig. 6B) and significantly decreased VEGFR3 expression (Fig. 6C).

Inhibition of DLL-class or JAG-class NOTCH signaling differentially regulated VEGFR1 expression. $N1_{1–13}$ and $N1_{1–24}$ decoys decreased *VEGFR1* transcripts. Conversely, $N1_{10–24}$ decoy or J1KD increased *VEGFR1* transcripts (Fig. 6D). However, VEGFR1 surface expression was not increased in $N1_{10–24}$ decoy or J1KD HUVEC (Fig. 6D). VEGFR1 exists as two splice variants that produce either a transmembrane receptor (VEGFR1) or a soluble protein (sVEGFR1/sFLT1). Using PCR primers specific for *sVEGFR1/sFLT1* transcripts, we found that $N1_{10–24}$ decoy or J1KD significantly increased *sVEGFR1/sFLT1* transcripts (Fig. 6E). The pan-ligand inhibitor $N1_{1–24}$ decoy also increased sVEGFR1/sFLT1 expression in HUVEC, though to a lesser degree (Fig. 6E). The *sVEGFR1/sFLT1* splice variant transcript levels were unaffected by DLL-specific $N1_{1–13}$ decoy (Fig. 6E). We validated these findings by ELISA using conditioned media from HUVECs expressing different N1 decoys, J1KD, or a constitutively signaling NOTCH1 intracellular domain (N1IC). The level of sVEGFR1/sFLT1 in the media was significantly increased with $N1_{10–24}$ and $N1_{1–24}$ decoys or JAG1 knockdown, and unaffected by $N1_{1–13}$ decoy or N1IC (Fig. 6F).

This complex regulation of VEGFR1/sFLT1 levels by JAG-mediated signaling was also seen in N1 decoy–treated tumors. A significant increase in VEGFR1/sFLT1 was observed in $N1_{10–24}$ and $N1_{1–24}$ decoy–treated Mm5MT-FGF4 tumors (Fig. 6G and H). A diffuse and nonvascular staining pattern observed in $N1_{10–24}$ and $N1_{1–24}$ decoy–treated tumors was indicative of increased soluble VEGFR1/sFLT1 (Fig. 6G). As sVEGFR1/sFLT1 functions as a competitive antagonist of VEGF–VEGFR2 signaling, the decrease in tumor angiogenesis we observed in the $N1_{10–24}$ and $N1_{1–24}$ decoy–treated tumors may arise due to decreased VEGFR2 signaling.

We investigated the role of sVEGFR1/sFLT1 as a downstream effector of JAG-induced NOTCH signaling. HUVECs were generated with *sVEGFR1/sFLT1* shRNA (sFLT1 KD) or scrambled shRNA (Scr), and N1 decoys or Fc, and the HUVEC bead sprouting angiogenesis assay was performed. $N1_{1–13}$ decoy/Scr HUVECs had increased branching relative to control, whereas $N1_{1–24}$ or $N1_{10–24}$ decoy/Scr or Fc/J1KD HUVECs had significantly reduced endothelial branching (Fig. 7A and B). Coexpression of *sFLT1* shRNA with $N1_{1–24}$, $N1_{10–24}$, or *JAG1* shRNA rescued endothelial branching inhibition elicited by JAG inhibition (Fig. 7A and B). sFLT1 knockdown consistently suppressed sFLT1 levels in HUVECs with JAG inhibitors to basal levels (Fig. 7C). These results demonstrate that the antiangiogenic effects of JAG blockade by either $N1_{1–24}$ decoy, $N1_{10–24}$ decoy, or *JAG1* shRNA likely result from an increase in sVEGFR1/sFLT1 secretion.

NOTCH1 Decoys Elicit Limited Gastrointestinal, Hepatic, and Renal Toxicity Compared with Gamma-Secretase Inhibition

Intestinal goblet cell hyperplasia occurs in mice treated with GSIs, or combined NOTCH1/NOTCH2 blockade (29, 31), and represents a potential dose-limiting toxicity of GSI use in the clinic. Our animal studies with $N1_{1–13}$, $N1_{1–24}$, or $N1_{10–24}$ decoys showed only a modest increase in goblet cell numbers, less than 2-fold, in the intestines of tumor-bearing mice, at the end of the 3-week experiment (Supplementary Fig. S9A and S9B). In contrast, GSI (compound E) treatment for only 5 days resulted in a 5-fold increase in goblet cells (Supplementary Fig. S9A and S9B). Consistent with this mild intestinal phenotype, weight loss was not observed in N1 decoy variant–expressing, tumor-bearing mice (Supplementary Fig. S9C). These results suggest that N1 decoy expression levels capable of eliciting antioncogenic activity do not cause significant intestinal toxicity.

We observed no significant effects on levels of markers of hepatic damage (Supplementary Fig. S10). Histopathologic analysis of the livers of mice infected with $N1_{1–13}$ decoy–expressing adenovirus demonstrated signs of minor sinusoidal dilation, whereas treatment with all other N1 decoys had no effect (Supplementary Fig. S11A). No changes in renal histomorphology were appreciable in any of the Fc- or N1 decoy–treated mice (Supplementary Fig. S11B). We conclude that NOTCH decoys represent a class of alternative NOTCH-targeting agents for antiangiogenic therapy with minimal gastrointestinal toxicities.

DISCUSSION

NOTCH proteins require EGF-like repeats 11 and 12 and calcium ions to interact productively with ligands (26, 32). Since the discovery of mammalian NOTCH1 (33), decades of study have yet to uncover domains of NOTCH that can distinguish JAG-class versus DLL-class ligand interactions. By fusing different regions of the NOTCH1 extracellular domain to human Fc, we developed NOTCH1 decoy proteins that selectively interact with either JAG- versus DLL-class NOTCH ligands and thus inhibit productive NOTCH signaling. Using NOTCH1 decoys, we discovered unique downstream signaling events in endothelial cells dependent on DLL- versus JAG-mediated NOTCH signaling. Specifically, DLL blockade reduced total VEGFR1 levels, whereas JAG blockade selectively increased the soluble splice variant sVEGFR1/sFLT1. The therapeutic potential of the NOTCH1 decoys was assessed in mouse tumor models, focusing on the effects on inhibiting

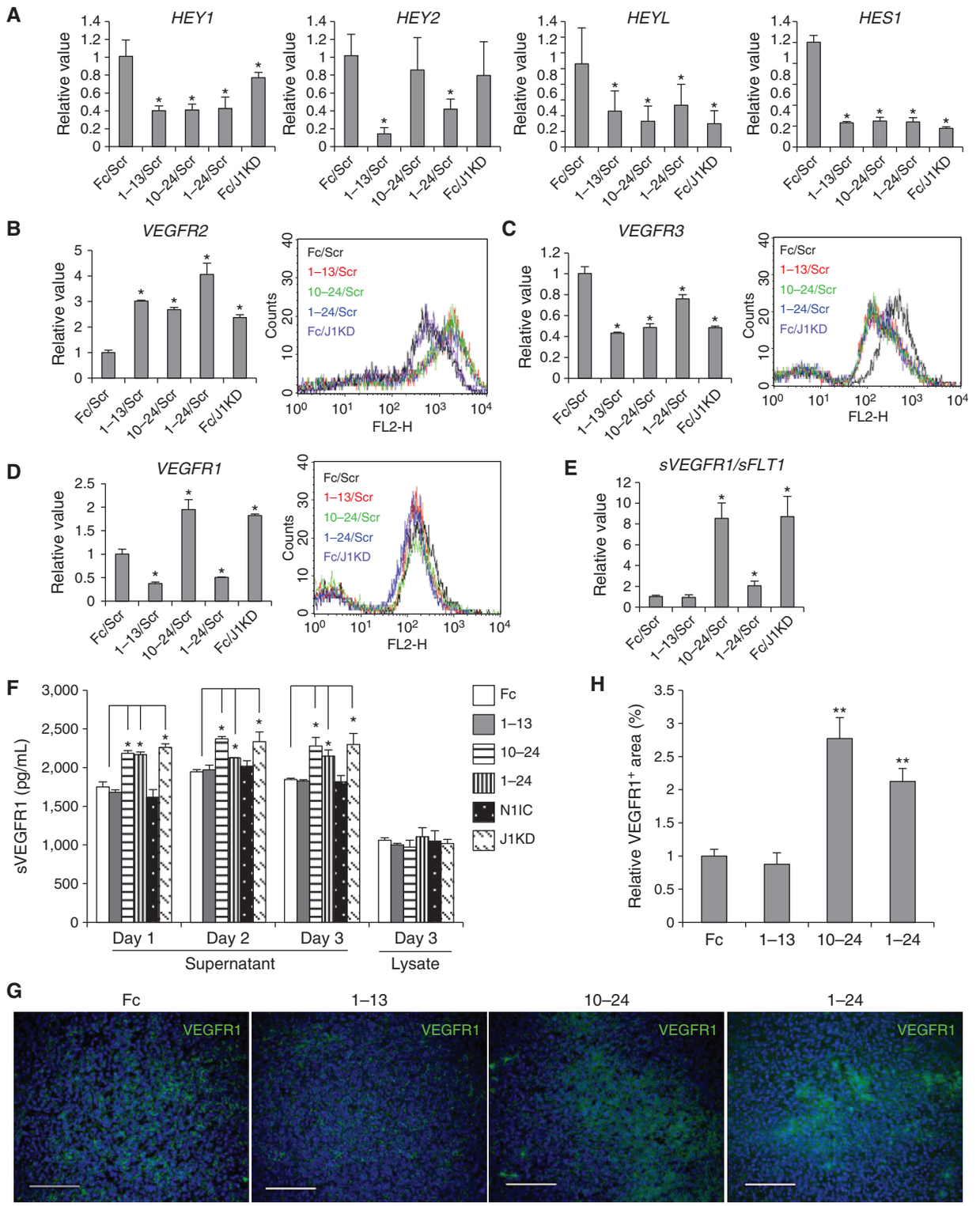

Figure 6. N1 decoys that block JAG elevate sVEGFR1/sFLT1. **A,** *HEY1*, *HEY2*, *HEYL*, and *HES1* qRT-PCR of N1 decoys or JAG1 knockdown (KD) HUVECs. **B–D,** VEGF receptor qRT-PCR and flow cytometry of N1 decoys or JAG1 KD HUVECs. **E,** soluble VEGFR1 (*sVEGFR1/sFLT1*) qRT-PCR of N1 decoys or JAG1 KD HUVECs. **A** to **E,** data, as ± SD; *, $P < 0.01$. **F,** soluble VEGFR1/sFLT1 ELISA presented as ± SD; *, $P < 0.02$. **G,** VEGFR1 staining of Mm5MT-FGF4 tumor sections; scale bars, 30 μm. **H,** quantitation of the percentage of the mean VEGFR1-positive area; **, $P < 0.001$ ($n = 3$).

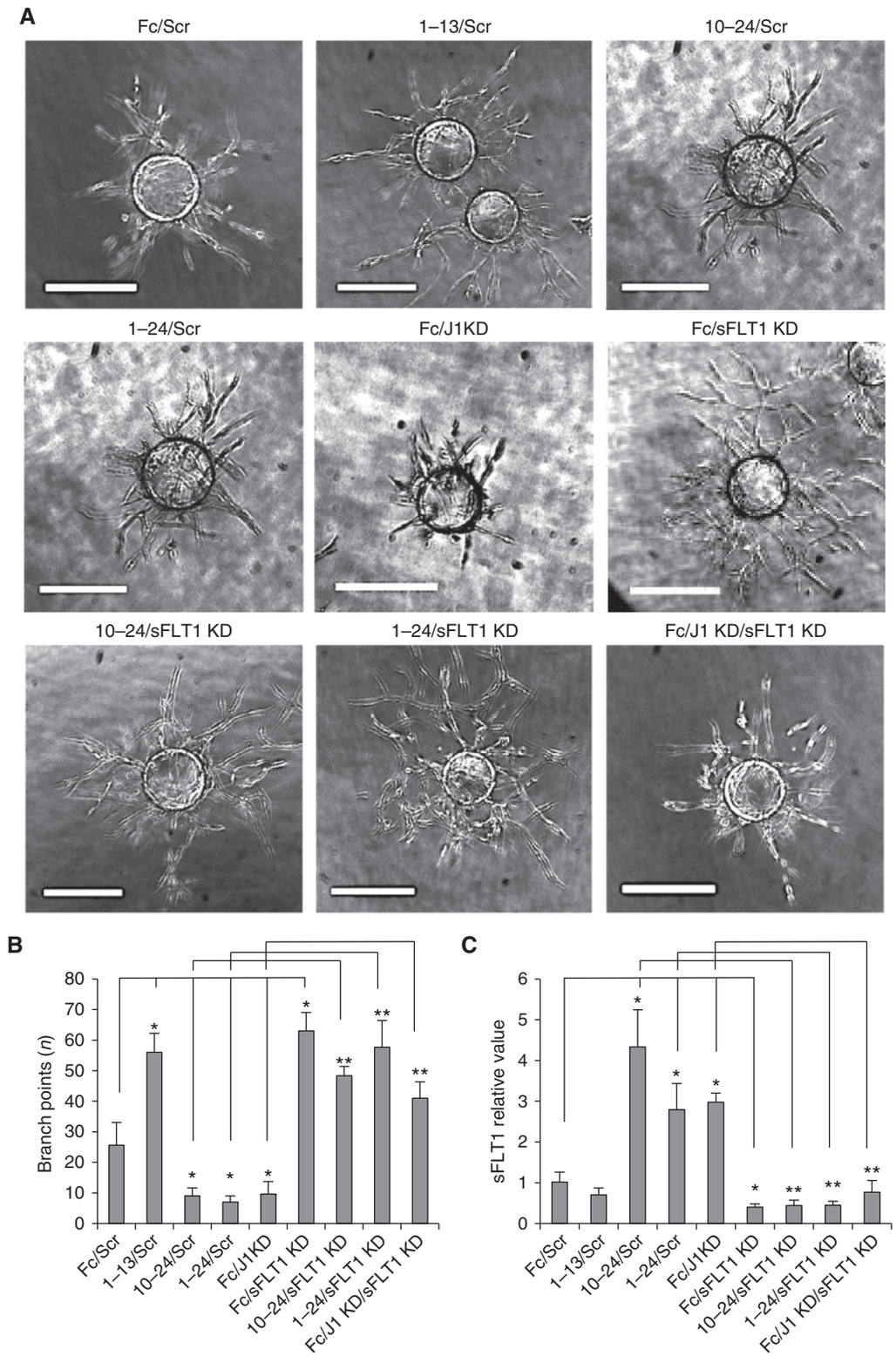

Figure 7. sVEGFR1/sFLT1 knockdown (KD) rescues antiangiogenic effects of N1 decoys that block JAG. **A,** day 7 assessment in the HUVEC capillary sprouting assay, using HUVECs transduced by different combinations of lentiviruses. Fc was used as control for N1 decoy overexpression, and scrambled shRNA (Scr) as control for sVEGFR1/sFLT1 or JAG1 (J1) KD; scale bars, 200 μm. **B,** quantification of the mean number of branch points per bead ± SD. **C,** *sVEGFR1/sFLT1* qRT-PCR ± SD. **B** and **C,** *, $P < 0.05$; **, $P < 0.005$. Fibrin bead sprouting assays were performed in triplicate.

DLL-class, JAG-class, or both classes of ligands. We found that all classes of ligand blockade inhibited tumor growth with minimal intestinal toxicity. Although both DLL-class and JAG-class NOTCH inhibitors disrupted tumor angiogenesis, they did so by distinct mechanisms. DLL/NOTCH blockade caused a hypersprouting phenotype resulting in dysfunctional, poorly perfused tumor vessels, whereas JAG/NOTCH blockade increased sVEGFR-1 levels, reducing tumor angiogenesis and perfusion. JAG/NOTCH blockade additionally disrupted pericyte association with the tumor endothelium. We conclude that blockade of JAG/NOTCH represents a distinct and novel therapeutic approach to inhibit tumor growth, resulting in reduced tumor angiogenesis and vessel functionality, while being tolerated by mice.

These studies shed new light on NOTCH signaling in the endothelium. We demonstrated that JAG–NOTCH and DLL–NOTCH signaling have overlapping and unique molecular targets in endothelial cells. Pan-ligand $N1_{1–24}$ decoy, DLL-specific $N1_{1–13}$ decoy, and JAG-specific $N1_{10–24}$ decoy all reduced the mRNA levels of NOTCH targets *HEY1*, *HEYL*, *HES1*, and *VEGFR3*, and increased *VEGFR2*, suggesting that these genes are targets of both DLL–NOTCH and JAG–NOTCH signaling. Analysis of NOTCH regulation of soluble VEGFR1/sFLT1, an antiangiogenic agent that functions as a decoy receptor for VEGF (34), revealed ligand-specific responses. DLL-specific $N1_{1–13}$ decoy reduced expression of *VEGFR1*, and this correlated with decreased expression of the NOTCH target and transcriptional repressor *HEY2*. JAG-specific $N1_{10–24}$ decoy increased *sVEGFR1/sFLT1* levels.

Unlike DLL4, the exact role of JAG1 in angiogenesis has been elusive. Endothelial JAG1 has been shown to reduce endothelial DLL4–NOTCH signaling when NOTCH is modified by Manic Fringe (24). In support of this model, endothelial-specific loss of JAG1 increased expression of NOTCH targets HEY1 and HES1 in the retinal endothelium and reduced retinal vascular density (24). Although consistent with previous studies where loss of endothelial JAG1 reduced retinal angiogenic sprouting (23, 24), the mechanism of action we uncovered demonstrates that JAG-class ligands can be positive effectors of endothelial NOTCH signaling and elicit a proangiogenic response. We found that JAG1 activates NOTCH signaling in endothelial cells to suppress sVEGFR1/sFLT1 levels, thus promoting angiogenesis. In fact, expression of $N1_{10–24}$ decoy suppressed sprouting angiogenesis *in vitro*, similar to that observed for JAG1 knockdown, which was reversed by using an *sVEGFR1/sFLT1* shRNA. This mechanism is consistent with the significant elevation of sVEGFR1/sFLT1 levels and reduced vascular density observed in tumors treated with $N1_{10–24}$ decoy. Thus, the antiangiogenic phenotype observed for JAG-specific NOTCH1 decoys in the *in vitro* sprouting assays and tumor xenografts is likely a result of increased levels of sVEGFR1/sFLT1.

Our studies do not exclude the possibility that JAG–NOTCH signaling may be both pro- and antiangiogenic and this may depend on the modification state of NOTCH. When JAG1 is an activating ligand, endothelial cells would respond by reducing sVEGFR1/sFLT1, whereas if NOTCH is modified by Manic Fringe and less responsive to JAG1, increased DLL4–NOTCH signaling would restrict sprouting and branch point formation. Thus, the particular role of endothelial JAG1 in angiogenesis is likely context dependent, differing based upon the levels and glycosylation state of endothelial NOTCH, or the cell-type presenting JAG1 to endothelial NOTCH. Tumor cells that overexpress JAG1 have been shown to promote tumor angiogenesis in mice (25, 35). Thus, tumor-derived JAG1 could serve as an angiogenic stimulus and may contribute to resistance to VEGF blockade. Selective inhibition of JAG-mediated NOTCH signaling is thus an important therapeutic approach to prevent tumor- or endothelial-derived JAG1 function.

JAG1-specific inhibition disrupted vascular mural cells associated with neonatal retinal and tumor vessels, revealing another role for JAG–NOTCH signaling in angiogenesis. $N1_{10–24}$ decoy reduced vascular smooth muscle cell coverage in arterioles of neonates and disrupted pericyte association with the tumor endothelium. Both observations are consistent with previous studies that showed that JAG1–NOTCH interactions are required for proper smooth muscle cell differentiation on arteries (23, 24). NOTCH regulates a wide range of signaling molecules that promote endothelial–mural cell interactions (36). Endothelial JAG1 signals to NOTCH3 in mural cells to promote vascular smooth muscle cell differentiation (37). Pericytes and vascular smooth muscle cells can produce VEGF-A, which is known to promote endothelial cell survival (38). We propose that deregulation of pericyte–endothelial interactions by JAG blockade contributes to vessel instability observed in tumors. The two major effects of $N1_{10–24}$ decoy on tumor vessels, disruption of tumor endothelial pericyte coverage and elevated sVEGFR1/sFLT1, have the combined effect of destabilizing tumor vessels and reducing VEGF–VEGFR2 signaling in tumor endothelium. We propose that this double antiangiogenic mechanism underlies the potent antitumor effect of JAG blockade.

The $N1_{1–13}$ decoy represents a therapeutic entity that functions similarly to DLL4-blocking antibodies. Blockade of DLL4/NOTCH leads to increased endothelial cell proliferation and increased tip cells, ultimately causing incomplete angiogenesis and poor vessel perfusion (5, 6, 28, 39). The DLL-specific $N1_{1–13}$ decoy identified EGF-like repeats 1 to 13 as critical for DLL-class ligand association and proved to function as a tumor inhibitor that resulted in poor vessel perfusion. $N1_{1–13}$ decoy caused elevation of VEGFR2 and a reduction of VEGFR1, a change that is proposed to underlie the hypersprouting phenotype caused by DLL4 blockade (40). Thus, the angiogenic phenotype of $N1_{1–13}$ decoy matched the biochemical activity predicted of a DLL4 inhibitor.

By developing N1 decoys that block both DLL- and JAG-class ligands and N1 decoys selective for each class, we were able to compare the effects of combined DLL and JAG blockade with ligand-class selective blockade. Similar to $N1_{10–24}$ decoy, $N1_{1–24}$ decoy blocked endothelial network formation during *in vitro* angiogenesis and increased sVEGFR1/sFLT1 levels in HUVEC cells, albeit not as strongly as $N1_{10–24}$ decoy. However, in retinal angiogenesis, treatment with the $N1_{1–24}$ decoy displayed a mixed phenotype. $N1_{1–24}$ decoy caused hypersprouting consistent with DLL4 blockade, but reduced mural cell coverage consistent with JAG blockade. In tumors, $N1_{1–24}$ decoy phenocopied $N1_{10–24}$ decoy in four different tumor models, causing reduced tumor vasculature and elevating sVEGFR1/sFLT1 in the Mm5MT tumor model. From these studies, we conclude that $N1_{1–24}$ decoy acts primarily as a JAG inhibitor in

the microenvironment of the assayed tumors. Of course, the phenotype caused by $N1_{1–24}$ decoy in any vascular bed, including those of tumors, will be dependent on the presence and activities of different NOTCH ligands and FRINGE proteins.

A major adverse effect of NOTCH blockade using GSIs (31) or combined NOTCH1/NOTCH2 blocking antibodies (29) is compromised gastrointestinal function. We found that $N1_{1–13}$, $N1_{10–24}$, $N1_{1–24}$ decoys were effective against four different tumor types and induced only minimal goblet cell metaplasia relative to GSI treatment, and were well tolerated by mice for 3 weeks, in which time GSI treatment could already be seen to cause adverse severe gastrointestinal effects. DLL4 blockade has also been found to have potential adverse events due to the hypersprouting in normal tissue vasculature (7). Consistent with this, we found that mice treated with the DLL-class inhibitor ($N1_{1–13}$ decoy) showed signs of minor hepatic angiogenic dysfunction in the form of dilated hepatic sinusoids, though this effect was slight and did not result in significant serum elevation of marker enzymes associated with hepatic damage. Conversely, the JAG-class $N1_{10–24}$ decoy and pan-ligand $N1_{1–24}$ decoy did not exhibit this effect on hepatic sinusoids. Furthermore, as the JAG-class inhibitor blocked angiogenesis, one may anticipate that hypersprouting in normal tissues will likely not occur with $N1_{10–24}$ decoy even with longer treatments. By developing a novel set of therapeutic agents that block either DLL- or JAG-class NOTCH ligands that are efficacious against tumors and lack severe toxicity in mice, the stage is set to advance NOTCH decoys for assessment in the clinic.

METHODS

Endothelial and Cancer Cell Lines

HUVECs isolated from human umbilical veins (IRB-AAAE4646) were grown in EGM-2 Media (Lonza). The HeLa, 293T, Mm5MT, LLC, CHO, and B16-F10 cells were obtained in 2008 from the ATCC, and KP1 from the Health Science Research Resource Bank in 2005. Cell lines were passaged for less than 5 months following resuscitation and were not authenticated. Cancer cells were maintained in DMEM, 10% FBS, and 100 U/mL of penicillin–streptomycin.

NOTCH Reporter Assay

pBOS–NOTCH1, pGL3–11CSL–Luc, and *Renilla* or either pCRIII–JAG1–FLAG, pCRIII–DLL4–FLAG, or pCRIII–GFP–FLAG were introduced to HeLa cells with Effectene (Qiagen). Twenty-four hours later, receptor- and ligand-expressing HeLa cells were cocultured in a 24-well plate. Luciferase activity was measured 24 hours after coculture, using the Dual-Luciferase Reporter Assay System (Promega). Assays were performed in triplicate.

Coimmunoprecipitation

N1 decoys and full-length DLL4–FLAG or JAG1–FLAG were cotransfected into 293T cells. Twenty-four hours after transfection, 20 nmol/mL of disuccinimidyl glutarate (Thermo Fisher Scientific) was added to the culture, incubated for 30 minutes, and quenched with 10 mmol/L Tris for 15 minutes. N1 decoy complexes were pulled down with Protein A/G Agarose and 50 μmol/mL of dithiothreitol was added to purified proteins and boiled for 5 minutes to reverse the crosslink.

Sprouting Angiogenesis Assay

The fibrin gel sprouting angiogenesis assay has been previously described (27). HUVECs were adhered to Cytodex 3 dextran beads (GE Healthcare Bio-Sciences Corp.) at 400 cells per bead and embedded in a fibrin clot composed of 2 mg/mL fibrinogen, 0.15 U/mL aprotinin, and 0.0625 U/mL thrombin (Sigma-Aldrich) in a 24-well plate. After 1 hour, Detroit 551 fibroblasts (ATCC) were seeded on top of the fibrin gel and cultures allowed to grow for 7 days. Experiments were performed in triplicate.

Mouse Husbandry

C57BL/6 mice and NCr nude mice were purchased from the NCI (Frederick, MD) and maintained in the barrier facility at the Irving Cancer Research Center at Columbia University. All mouse studies were performed in accordance with the Guide for the Care and Use of Laboratory Animals of the National Institutes of Health and were approved by the Institutional Animal Care and Use Committee of Columbia University (protocols AC-AAAB8961 and AC-AAAD3700).

Retinal Analysis

C57BL/6 mice postnatal day 2 (P2) pups were s.c. injected with 2.5×10^8 focus forming unit (ffu) adenoviruses encoding N1 decoys or Fc. Eyes were isolated at P5 and fixed in 4% paraformaldehyde (PFA). For adults, 5×10^8 ffu N1 decoy adenovirus was administered via retro-orbital i.v. injection to 4- to 6-week-old female NCr nude mice, and eyes were isolated 21 days later. Dissected retinas were permeabilized with 1% BSA and 0.5% Triton X-100 in 1x PBS at room temperature for 2 hours and subsequently washed three times in PBLEC buffer (1%Triton X-100, 0.1 mmol/L $MgCl_2$, 0.1 mmol/L $CaCl_2$, 0.1 mmol/L $MnCl_2$ in 1x PBS pH6.8). For immunofluorescence, retinas were incubated with Biotin-conjugated isolectin B4 (Vector Laboratories) detected with streptavidin-conjugated Alexa Fluor 488 (Invitrogen), and Cy3-conjugated αSMA (Sigma-Aldrich) washed with PBLEC, post-fixed with 4% PFA, and mounted. Images were acquired using a laser scanning confocal Zeiss LSM 510 Meta microscope and LSM software.

Quantitative Real-Time PCR

RNA was collected using the RNeasy Mini Kit (Qiagen) and treated with DNase I for 30 minutes, and cDNA was synthesized with the SuperScript First-Strand Synthesis System for RT-PCR (Invitrogen). PCR reactions were done with Absolute Blue QPCR SYBR Green Mix (Thermo Fisher Scientific).

Tumor Experiment

Mm5MT-FGF4 cells (1.0×10^5), KP1-VEGF cells (2.0×10^6), LLC cells (5.0×10^5), or B16-F10 cells (5.0×10^5) were s.c. implanted into the upper flank of 4- to 6-week-old female NCr nude mice. Three days later, 5×10^8 ffu N1 decoy adenovirus was administered via retro-orbital i.v. injection. Tumors were harvested and weighed at day 21. To measure hypoxia, 60 mg/kg hypoxyprobe-1 (Hypoxyprobe, Inc.) was injected i.p. 30 minutes before sacrifice, and sections were immunostained with an anti-hypoxyprobe antibody. To assess vessel perfusion, 100 μg of fluorescein *Lycopersicon esculentum* lectin (Vector Laboratories) was intracardiac injected into the left ventricle, and mice were perfused with 1% PFA after 2 minutes. Lectin bound to the endomucin-positive endothelial cell surface was scored as a perfused vessel.

Tissue Analysis in Mice Expressing N1 Decoys

For intestinal toxicity, duodena were harvested at the time of tumor harvest. For renal and liver toxicity, adenovirus was retro-orbitally administered to 4- to 6-week-old NCr nude mice, and serum and tissue were harvested after 21 days. Duodena and kidney sections were Periodic Acid–Schiff stained. Liver sections were stained by hematoxylin and eosin. Serum was sent for liver panel analysis to ANTECH Diagnostics. Statistical analyses were performed using the nonparametric *T* test or one-way ANOVA, as indicated.

Immunofluorescent Staining

Fresh-frozen 7-μm tumor sections were incubated with primary antibodies: endomucin (Santa Cruz Biotechnology), NG2 (Millipore), αSMA (Sigma-Aldrich), collagen IV (COSMO bio), and VEGFR1 (Abcam). Alexa Fluor–conjugated 588 or 594 secondary antibodies (Invitrogen) were used and slides mounted with Vectashield with DAPI (Vector Laboratories).

ELISA/FACS

sVEGFR1 ELISA was performed with the Human sVEGFR1/FLT1 Quantikine ELISA Kit (R&D Systems). VEGFR1/2/3 FACS was performed with Monoclonal Anti-Human VEGF Receptor Phycoerythrin Sampler Pack (R&D Systems).

Disclosure of Potential Conflicts of Interest

T. Kangsamaksin has ownership interest in a human NOTCH1 decoys patent. C.J. Shawber reports receiving commercial research support from Eisai. J. Kitajewski reports receiving a commercial research grant from Eisai. No potential conflicts of interest were disclosed by the other authors.

Authors' Contributions

Conception and design: T. Kangsamaksin, N.M. Kofler, H. Cuervo, R.A. Chaudhri, I.W. Tattersall, C.J. Shawber, J. Kitajewski
Development of methodology: T. Kangsamaksin, R.A. Chaudhri, I.W. Tattersall, C.J. Shawber
Acquisition of data (provided animals, acquired and managed patients, provided facilities, etc.): T. Kangsamaksin, A. Murtomaki, H. Cuervo, R.A. Chaudhri, I.W. Tattersall
Analysis and interpretation of data (e.g., statistical analysis, biostatistics, computational analysis): T. Kangsamaksin, H. Cuervo, R.A. Chaudhri, P.E. Rosenstiel, J. Kitajewski
Writing, review, and/or revision of the manuscript: T. Kangsamaksin, A. Murtomaki, H. Cuervo, R.A. Chaudhri, I.W. Tattersall, C.J. Shawber, J. Kitajewski
Administrative, technical, or material support (i.e., reporting or organizing data, constructing databases): N.M. Kofler, R.A. Chaudhri
Study supervision: C.J. Shawber, J. Kitajewski
Other (design, development, and acquisition of data presented in response to reviewer comments): I.W. Tattersall

Acknowledgments

The authors thank Anshula Sharma and Valeriya Borisenko for technical support and Minji Kim Uh for advice on this article.

Grant Support

This work was supported by grants NIH/NCI R01CA136673 (to J. Kitajewski and C.J. Shawber) and NIH/NHLBI RO1HL062454 (to J. Kitajewski), and funding from Eisai Incorporated (to J. Kitajewski).

The costs of publication of this article were defrayed in part by the payment of page charges. This article must therefore be hereby marked *advertisement* in accordance with 18 U.S.C. Section 1734 solely to indicate this fact.

Received June 23, 2014; revised November 4, 2014; accepted November 7, 2014; published OnlineFirst November 11, 2014.

REFERENCES

1. Hellström M, Phng L-K, Hofmann JJ, Wallgard E, Coultas L, Lindblom P, et al. Dll4 signalling through Notch1 regulates formation of tip cells during angiogenesis. Nature 2007;445:776–80.
2. Lobov IB, Renard RA, Papadopoulos N, Gale NW, Thurston G, Yancopoulos GD, et al. Delta-like ligand 4 (Dll4) is induced by VEGF as a negative regulator of angiogenic sprouting. Proc Natl Acad Sci U S A 2007;104:3219–24.
3. Suchting S, Freitas C, Le Noble F, Benedito R, Bréant C, Duarte A, et al. The Notch ligand Delta-like 4 negatively regulates endothelial tip cell formation and vessel branching. Proc Natl Acad Sci U S A 2007;104:3225–30.
4. Kalén M, Heikura T, Karvinen H, Nitzsche A, Weber H, Esser N, et al. Gamma-secretase inhibitor treatment promotes VEGF-a-driven blood vessel growth and vascular leakage but disrupts neovascular perfusion. PLoS ONE 2011;6:e18709.
5. Ridgway J, Zhang G, Wu Y, Stawicki S, Liang W-C, Chanthery Y, et al. Inhibition of Dll4 signalling inhibits tumour growth by deregulating angiogenesis. Nature 2006;444:1083–7.
6. Noguera-Troise I, Daly C, Papadopoulos NJ, Coetzee S, Boland P, Gale NW, et al. Blockade of Dll4 inhibits tumour growth by promoting non-productive angiogenesis. Nature 2006;444:1032–7.
7. Yan M, Callahan CA, Beyer JC, Allamneni KP, Zhang G, Ridgway JB, et al. Chronic DLL4 blockade induces vascular neoplasms. Nature 2010;463:E6–7.
8. Kopan R, Ilagan MXG. The canonical Notch signaling pathway: unfolding the activation mechanism. Cell 2009;137:216–33.
9. Glittenberg M, Pitsouli C, Garvey C, Delidakis C, Bray S. Role of conserved intracellular motifs in Serrate signalling, cis-inhibition, and endocytosis. EMBO J 2006;25:4697–706.
10. Henderson ST, Gao D, Christensen S, Kimble J. Functional domains of LAG-2, a putative signaling ligand for LIN-12 and GLP-1 receptors in Caenorhabditis elegans. Mol Biol Cell 1997;8:1751–62.
11. Cordle J, Johnson S, Tay JZY, Roversi P, Wilkin MB, de Madrid BH, et al. A conserved face of the Jagged/Serrate DSL domain is involved in Notch trans-activation and cis-inhibition. Nat Struct Mol Biol 2008;15:849–57.
12. Hambleton S, Valeyev NV, Muranyi A, Knott V, Werner JM, McMichael AJ, et al. Structural and functional properties of the human notch-1 ligand binding region. Structure 2004;12:2173–83.
13. Ranganathan P, Weaver KL, Capobianco AJ. Notch signalling in solid tumours: a little bit of everything but not all the time. Nat Rev Cancer 2011;11:338–51.
14. Takebe N, Warren RQ, Ivy SP. Breast cancer growth and metastasis: interplay between cancer stem cells, embryonic signaling pathways and epithelial-to-mesenchymal transition. Breast Cancer Res 2011;13:211.
15. Thurston G, Kitajewski J. VEGF and Delta-Notch: interacting signalling pathways in tumour angiogenesis. Br J Cancer 2008;99:1204–9.
16. Liu Z-J, Shirakawa T, Li Y, Soma A, Oka M, Dotto GP, et al. Regulation of Notch1 and Dll4 by vascular endothelial growth factor in arterial endothelial cells: implications for modulating arteriogenesis and angiogenesis. Mol Cell Biol 2003;23:14–25.
17. Patel N, Li J, Generali D, Poulsom R, Cranston D, Harris A. Up-regulation of delta-like 4 ligand in human tumor vasculature and the role of basal expression in endothelial cell function. Cancer Res 2005;65:8690–7.
18. Funahashi Y, Shawber CJ, Sharma A, Kanamaru E, Choi YK, Kitajewski J. Notch modulates VEGF action in endothelial cells by inducing Matrix Metalloprotease activity. Vascular Cell 2011;3:2.
19. Taylor KL, Henderson AM, Hughes CCW. Notch activation during endothelial cell network formation *in vitro* targets the basic HLH transcription factor HESR-1 and downregulates VEGFR-2/KDR expression. Microvasc Res 2002;64:372–83.
20. Shawber CJ, Funahashi Y, Francisco E, Vorontchikhina M, Kitamura Y, Stowell SA, et al. Notch alters VEGF responsiveness in human and murine endothelial cells by direct regulation of VEGFR-3 expression. J Clin Invest 2007;117:3369–82.
21. Geudens I, Herpers R, Hermans K, Segura I, Ruiz de Almodovar C, Bussmann J, et al. Role of delta-like-4/Notch in the formation and wiring of the lymphatic network in zebrafish. Arterioscler Thromb Vasc Biol 2010;30:1695–702.
22. Tammela T, Zarkada G, Nurmi H, Jakobsson L, Heinolainen K, Tvorogov D, et al. VEGFR-3 controls tip to stalk conversion at vessel fusion sites by reinforcing Notch signalling. Nat Cell Biol 2011;13:1202–13.

23. High FA, Lu MM, Pear WS, Loomes KM, Kaestner KH, Epstein JA. Endothelial expression of the Notch ligand Jagged1 is required for vascular smooth muscle development. Proc Natl Acad Sci U S A 2008;105:1955–9.
24. Benedito R, Roca C, Sörensen I, Adams S, Gossler A, Fruttiger M, et al. The notch ligands Dll4 and Jagged1 have opposing effects on angiogenesis. Cell 2009;137:1124–35.
25. Funahashi Y, Hernandez SL, Das I, Ahn A, Huang J, Vorontchikhina M, et al. A notch1 ectodomain construct inhibits endothelial notch signaling, tumor growth, and angiogenesis. Cancer Res 2008;68:4727–35.
26. Rebay I, Fleming R, Fehon R, Cherbas L, Cherbas P, Artavanis-Tsakonas S. Specific EGF repeats of Notch mediate interactions with Delta and Serrate: implications for Notch as a multifunctional receptor. Cell 1991;67:687–99.
27. Nakatsu MN, Hughes CC. An optimized three-dimensional *in vitro* model for the analysis of angiogenesis. Methods Enzymol 2008;443:65–82.
28. Li J-L, Sainson RCA, Shi W, Leek R, Harrington LS, Preusser M, et al. Delta-like 4 Notch ligand regulates tumor angiogenesis, improves tumor vascular function, and promotes tumor growth *in vivo*. Cancer Res 2007;67:11244–53.
29. Wu Y, Cain-Hom C, Choy L, Hagenbeek TJ, de Leon GP, Chen Y, et al. Therapeutic antibody targeting of individual Notch receptors. Nature 2010;464:1052–7.
30. Nakagawa O, McFadden DG, Nakagawa M, Yanagisawa H, Hu T, Srivastava D, et al. Members of the HRT family of basic helix-loop-helix proteins act as transcriptional repressors downstream of Notch signaling. Proc Natl Acad Sci U S A 2000;97:13655–60.
31. van Es JH, van Gijn ME, Riccio O, van den Born M, Vooijs M, Begthel H, et al. Notch/gamma-secretase inhibition turns proliferative cells in intestinal crypts and adenomas into goblet cells. Nature 2005;435:959–63.
32. Rand MD, Grimm LM, Artavanis-Tsakonas S, Patriub V, Blacklow SC, Sklar J, et al. Calcium depletion dissociates and activates heterodimeric notch receptors. Mol Cell Biol 2000;20:1825–35.
33. Weinmaster G, Roberts VJ, Lemke G. A homolog of Drosophila Notch expressed during mammalian development. Development 1991;113:199–205.
34. Shibuya M. Vascular endothelial growth factor receptor-1 (VEGFR-1/Flt-1): a dual regulator for angiogenesis. Angiogenesis 2006;9:225–30.
35. Zeng Q, Li S, Chepeha D, Giordano T, Li J, Zhang H, et al. Crosstalk between tumor and endothelial cells promotes tumor angiogenesis by MAPK activation of Notch signaling. Cancer Cell 2005;8:13–23.
36. Armulik A, Abramsson A, Betsholtz C. Endothelial/pericyte interactions. Circ Res 2005;97:512–23.
37. Domenga V, Fardoux P, Lacombe P, Monet M, Maciazek J, Krebs LT, et al. Notch3 is required for arterial identity and maturation of vascular smooth muscle cells. Genes Dev 2004;18:2730–5.
38. Franco M, Roswall P, Cortez E, Hanahan D, Pietras K. Pericytes promote endothelial cell survival through induction of autocrine VEGF-A signaling and Bcl-w expression. Blood 2011;118:2906–17.
39. Hoey T, Yen W-C, Axelrod F, Basi J, Donigian L, Dylla S, et al. DLL4 blockade inhibits tumor growth and reduces tumor-initiating cell frequency. Cell Stem Cell 2009;5:168–77.
40. Potente M, Gerhardt H, Carmeliet P. Basic and therapeutic aspects of angiogenesis. Cell 2011;146:873–87.